Electronic Supplementary Material (ESI) for Environmental Science: Nano.
This journal is © The Royal Society of Chemistry 2022

Supplementary data

Yolk–shell-type gold nanosphere-encapsulated mesoporous silica for catalytic oxidation of organic pollutants in the presence of persulfate

Geun Young Kim,[a,†] Donghyun Lee,[b,†] Hyun-Seok Choe,[a] Jeong-Min Park,[a] Suyoung Jeong,[a] Erwin Jongwoo Park,[b] Ji Won Lee,[b] Changha Lee[b,*] and Jae-Hyuk Kim[a,*]

[a]Department of Civil and Environmental Engineering, Pusan National University, 2, Busandaehak-ro 63beon-gil, Geumjeong-gu, Busan, 46241, Republic of Korea

[b]School of Chemical and Biological Engineering, Institute of Chemical Process (ICP), Seoul National University, 1 Gwanak-ro, Gwanak-gu, Seoul, 08826, Republic of Korea

***Corresponding Author:** Jae-Hyuk Kim, Ph.D., Department of Civil and Environmental Engineering, Pusan National University, Busan 46241, Republic of Korea. Tel.: 82-51-510-2312. E-mail: jaehyuk.kim@pusan.ac.kr; Changha Lee, Ph.D., School of Chemical and Biological Engineering, Institute of Chemical Process (ICP), Seoul National University, 1 Gwanak-ro, Gwanak-gu, Seoul 08826, Republic of Korea. Tel.: 82-2-880-8630. E-mail: leechangha@snu.ac.kr

†These authors have contributed equally to this work

Text S1. Analytical condition of LC/MS.

The oxidation intermediates were analyzed by a ultra-high performance liquid chromatograph (Vanquish UHPLC) coupled with quadrupole orbitrap mass spectrometry (Q Exactive Orbitrap MS). The separation was performed with Water Cortecs C18 column (150 × 2.1, 1.63 um) with the column temperature 45°C. 0.1% of formic acid (A) and methanol (B) were used as the eluent at a flow rate of 0.25 mL/min and the elution gradient was as follows: A:B = 95:5 for 0-0.5 min, A:B = 80:20 for 0.5-7 min, A:B = 5:95 for 7-10 min, A:B = 5:95 for 10-11 min and A:B = 95:5 for 11.1-15 min. The heated electrospray ionization source interface was operated in the negative ionization mode with following conditions: spray voltage =3500 V, capillary temperature = 320°C, spray current = 28 µA, sheath gas flow rate =50 arbitrary units, auxiliary gas flow rate =10 arbitrary units, sweep gas flow rate =1 arbitrary units, S-lens RF level =50. The full scan mode analysis was conducted with a scan range from 50 to 200 m/z.

No.	Catalyst	Pollutant concentration	Catalyst dosage (g/L)	Oxidant dosage	Reaction time (min)	Degradation efficiency (%)	Ref.
1	Yolk–shell Co/C nanoreactor/ PMS	20 mg/L (BPA)	0.1	0.15 g/L (PMS)	15	100	[S1]
2	Yolk–shell Co_3O_4@MOFs/ PMS	0.78 mM (4-chlorophenol)	0.5	0.8 mM (PMS)	150	100	[S2]
3	Co/N/S-doped yolk–shell carbon/PMS	60 mg/L (4-nitrophenol)	0.1	0.2 g/L (PMS)	30	98	[S3]
4	AuNS@$_y$SiO$_2$/ PDS	0.5 mM (phenol)	2.0	10 mM (PDS)	20	100	This study

Table S1. Comparison of degradation efficiency of yolk–shell-structured catalysts.

Table S2. Comparison of PDS-utilization efficiency.

No.	Catalytic system	Pollutant concentration	Catalyst dosage	PDS dosage	PDS utilization efficiency	Ref.
1	nFe^0/PDS	0.1 mM (4-chlorophenol)	0.05 g/L	1 mM	8%	[S4]
2	Carbon nanotube/PDS	0.1 mM (4-chlorophenol)	0.1 g/L	1 mM	83%	[S4]
3	CuO-gFe_2O_3/PDS	20 mg/L (Acid orange)	0.6 g/L	0.8 g/L	90.8%	[S5]
4	Co_3O_4-CeO_2/PDS	20 mg/L (Diclofenac)	1.0 g/L	0.1 g/L	20%	[S6]
5	Graphitized nanodiamonds/ PDS	0.01 mM (Phenol)	0.1 g/L	1 mM	3.5%	[S7]
6	Nanodiamonds -2000/PDS	0.1 mM (4-chlorophenol)	0.05 g/L	0.5 mM	89.5%	[S8]
7	CuO/MgO hybrid/PDS	0.2 mM (Bisphenol A)	0.18 g/L	0.2 mM	37.3%	[S9]
8	$AuNS@_ySiO_2$/ PDS	0.5 mM (Phenol)	2.0 g/L	10 mM	93.2%	This study

Table S3. Cumulative concentration of gold ions leached during repeated degradation processes ([phenol]$_0$ = 0.10 mM; [PDS]$_0$ = 10.0 mM; [AuNS@$_y$SiO$_2$]$_0$ = 2.0 g/L; pH = 3.0; reaction time = 40 min)

	Cycle	**Concentration of leached gold ions (μg/L)**	**Cumulative concentration of leached gold ions (μg/L)**
AuNS@$_y$SiO$_2$	1st cycle	0.509	0.509
	2nd cycle	N.D.*	0.509
	3rd cycle	0.0345	0.5435
	4th cycle	1.8575	2.401
	5th cycle	1.333	3.734

*: Not detected.

Table S4. Second-order rate constants for the reactions of reactive oxidants with various radical scavengers

Scavenger	Radical species	Rate constant, *k* ($M^{-1}s^{-1}$)	Reference
Methanol	$^{\bullet}OH$	$k_{OH^{\bullet}} = 9.7 \times 10^{8}$	[S10, S11]
	$SO_4^{\bullet-}$	$k_{SO_4^{\bullet-}} = 3.2 \times 10^{6}$	
TBA	$^{\bullet}OH$	$k_{OH^{\bullet}} = 3.8 \times 10^{8}–7.6 \times 10^{8}$	[S10]
	$SO_4^{\bullet-}$	$k_{SO_4^{\bullet-}} = 4 \times 10^{5}–9.1\times 10^{5}$	[S12]
DMSO	$^{\bullet}OH$	$k_{OH^{\bullet}} = 6.6 \times 10^{9}$	[S10]
	$SO_4^{\bullet-}$	$k_{SO_4^{\bullet-}} = 3.0\times 10^{9}$	[S13]

Table S5. Second-order rate constants for the reactions of $^{\bullet}OH$, $SO_4^{\bullet-}$, and $^1O_2$ with various organic pollutants

Organic pollutants	**Reactive species**	**Rate constant, *k* ($M^{-1}s^{-1}$)**	**Reference**
Phenol	$^{\bullet}OH$	$k_{^{\bullet}OH} = 6.6 \times 10^9$	[S10] [S14, S15]
	$SO_4^{\bullet-}$	$k_{so_4^{\bullet-}} = 8.8 \times 10^9$	
	$^1O_2$	$k_{^1O_2} = 2 \times 10^6$–$3 \times 10^6$	
Benzoic acid	$^{\bullet}OH$	$k_{^{\bullet}OH} = 4.3 \times 10^9$	[S10] [S12]
	$SO_4^{\bullet-}$	$k_{so_4^{\bullet-}} = 1.2 \times 10^9$	
Furfuryl alcohol	$^{\bullet}OH$	$k_{^{\bullet}OH} = 1.5 \times 10^{10}$	[S10] [S15]
	$^1O_2$	$k_{^1O_2} = 1.2 \times 10^8$	
Atrazine	$^{\bullet}OH$	$k_{^{\bullet}OH} = 2.25 \times 10^9$	[S16]
	$SO_4^{\bullet-}$	$k_{so_4^{\bullet-}} = 2.59 \times 10^9$	
Sulfamethoxazole	$^{\bullet}OH$	$k_{^{\bullet}OH} = 4.3 \times 10^9$	[S17]
	$SO_4^{\bullet-}$	$k_{so_4^{\bullet-}} = 6.6 \times 10^9$–$11.8 \times 10^9$	[S18]

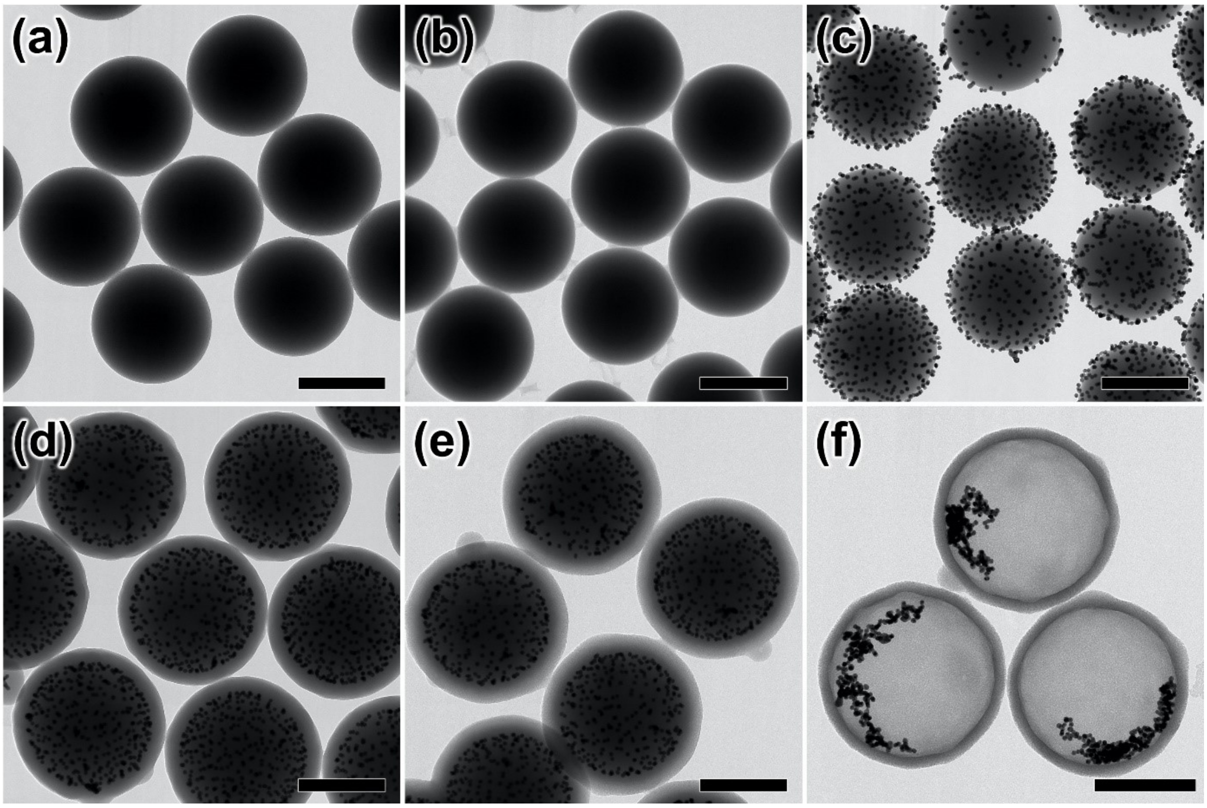

Fig. S1. Low-magnification TEM images of (a) $_{s}SiO_2$, (b) $_{s}SiO_2$-NH_2, (c) $_{s}SiO_2$@AuNS, (d) $_{s}SiO_2$@AuNS@$_{s}SiO_2$, (e) $_{s}SiO_2$@AuNS@$_{s}SiO_2$@$_{o}SiO_2$, and (f) AuNS@$_{y}SiO_2$. All scale bars represent 300 nm.

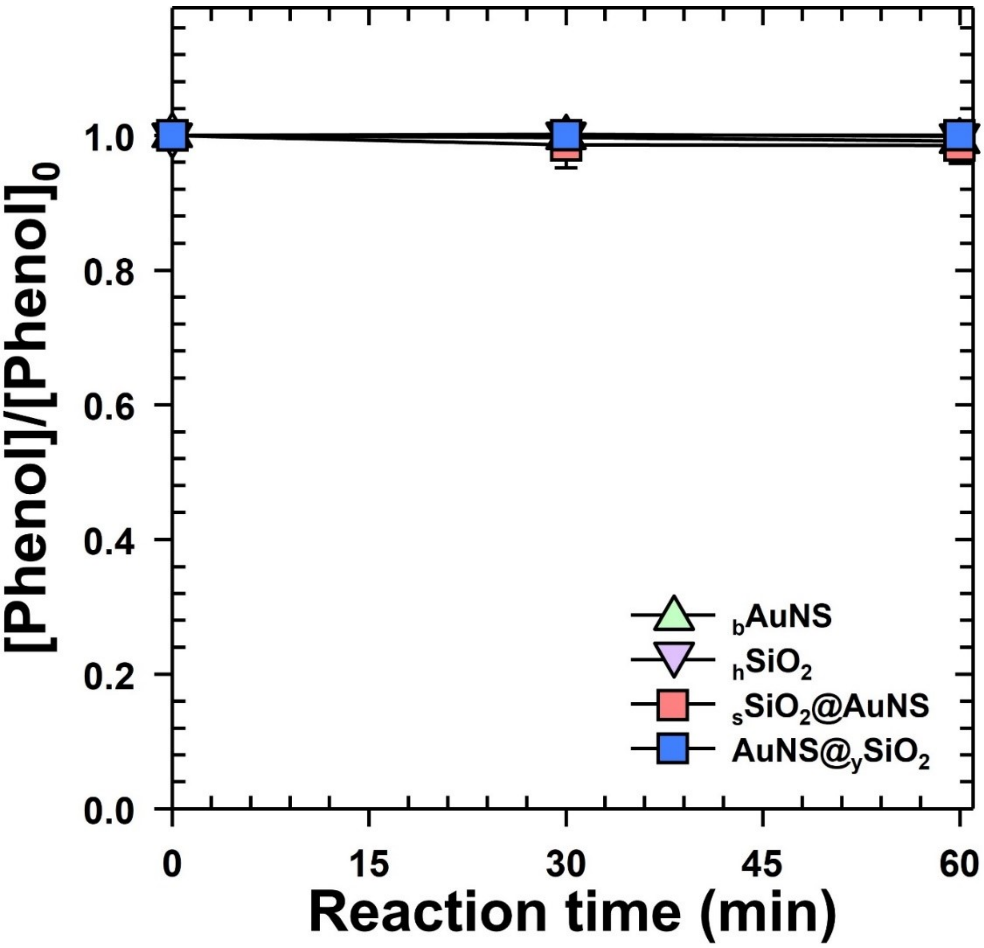

Fig. S2. Adsorption of phenol by $_b$AuNS, $_h$SiO$_2$, $_s$SiO$_2$@AuNS, and AuNS@$_y$SiO$_2$. ([phenol]$_0$ = 0.50 mM; [$_b$AuNS]$_0$ = 0.76 g/L, [$_h$SiO$_2$]$_0$ = 1.4 g/L, [$_s$SiO$_2$@AuNS]$_0$ = 7.2 g /L, [AuNS@$_y$SiO$_2$]$_0$ = 2.0 g/L; pH = 3.0; reaction time = 60 min).

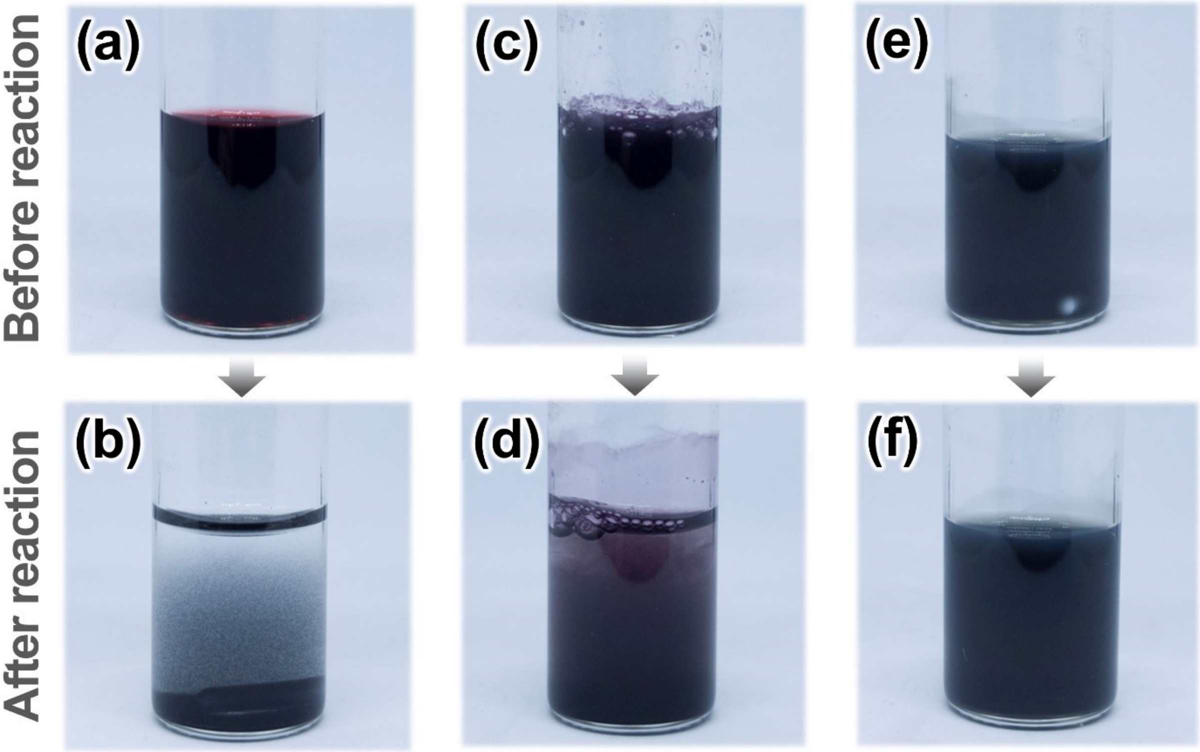

Fig. S3. Photographs captured before and after PDS treatment of: (a and b) $_b$AuNS, (c and d) $_s$SiO$_2$@AuNS, and (e and f) AuNS@$_y$SiO$_2$ ([phenol]$_0$ = 1.5 mM; [PDS]$_0$ = 30.0 mM; [$_b$AuNS]$_0$ = 0.76 g/L, [$_s$SiO$_2$@AuNS]$_0$ = 7.2 g /L, [AuNS@$_y$SiO$_2$]$_0$ = 2.0 g/L; pH = 3.0; reaction time = 60 min).

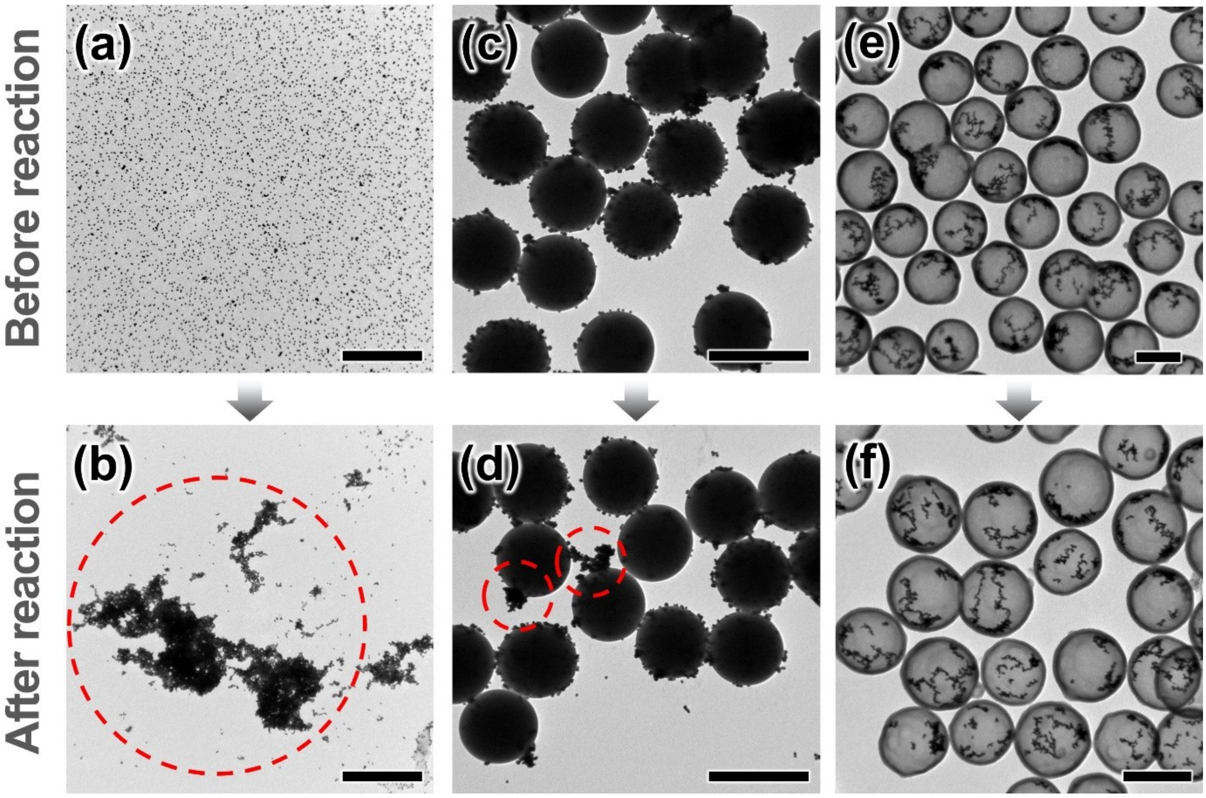

Fig. S4. TEM images of before and after PDS treatment for (a and b) $_b$AuNS, (c and d) $_s$SiO$_2$@AuNS, and (e and f) AuNS@$_y$SiO$_2$. Scale bars in (a−d) and (e and f) represent 1 μm and 500 nm, respectively. ([phenol]$_0$ = 1.5 mM; [PDS]$_0$ = 30.0 mM; [$_b$AuNS]$_0$ = 0.76 g/L, [$_s$SiO$_2$@AuNS]$_0$ = 7.2 g /L, [AuNS@$_y$SiO$_2$]$_0$ = 2.0 g/L; pH = 3.0; reaction time = 60 min).

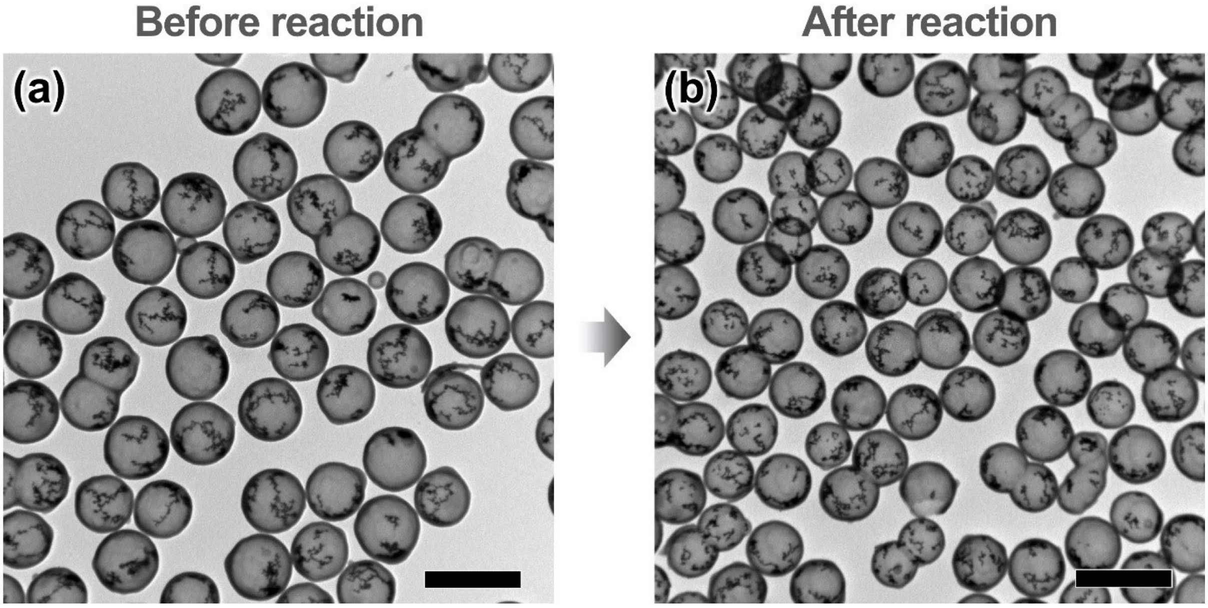

Fig. S5. TEM images of AuNS@$_y$SiO$_2$ (a) before (initial) and (b) after (5th cycle) PDS treatment. All scale bars represent 1 μm. ([phenol]$_0$ = 0.10 mM; [PDS]$_0$ = 10.0 mM; [AuNS@$_y$SiO$_2$]$_0$ = 2.0 g/L; pH = 3.0; reaction time = 40 min).

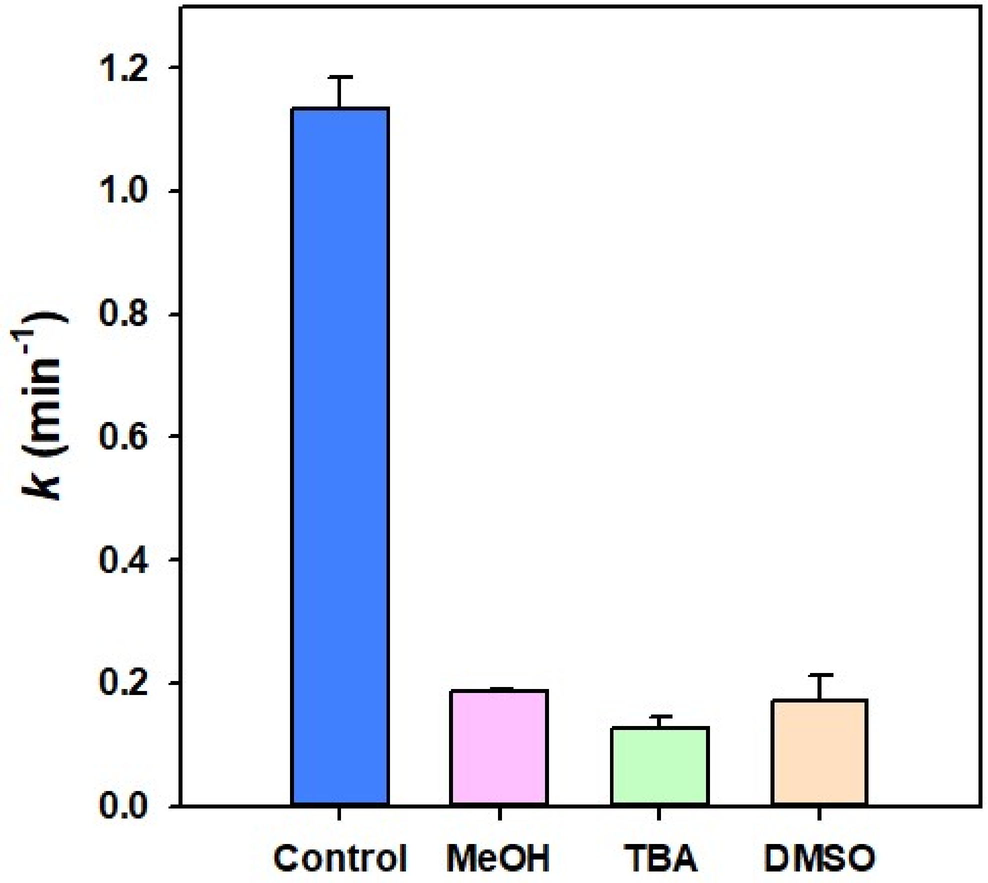

Fig. S6. Kinetic rates of phenol degradation in the presence of excess scavengers ($[\text{phenol}]_0$ = 0.50 mM; $[\text{PDS}]_0$ = 10.0 mM; $[\text{MeOH}]_0 = [\text{TBA}]_0 = [\text{DMSO}]_0$ = 100 mM; $[\text{AuNS@}_y\text{SiO}_2]_0$ = 2.0 g/L; pH = 3.0; reaction time = 20 min).

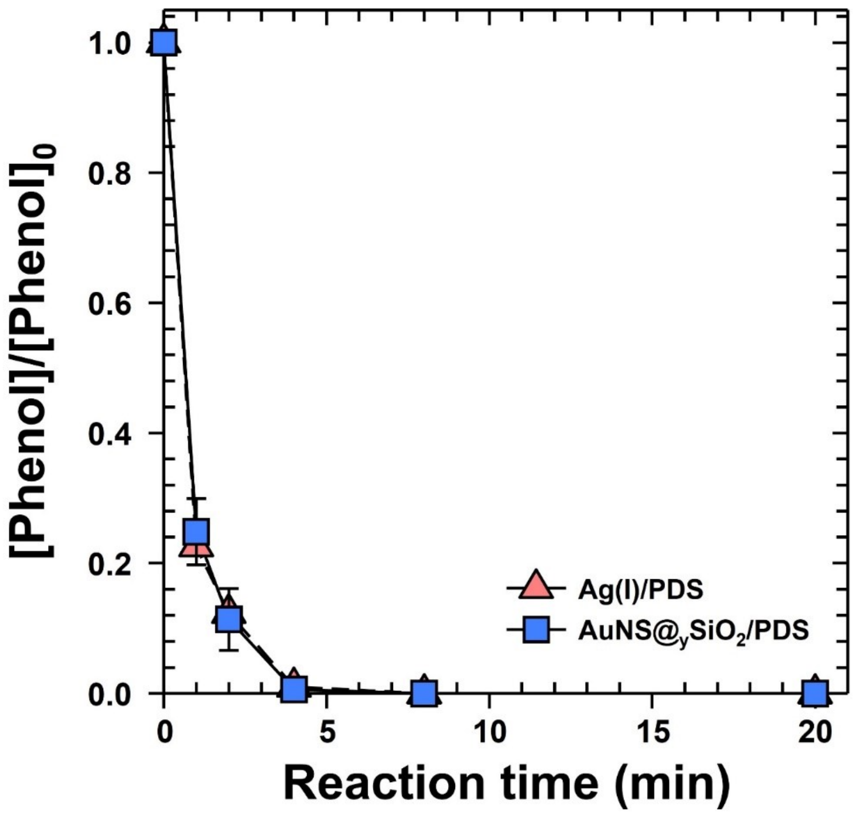

Fig. S7. Degradation of phenol by the Ag(I)/PDS system and the AuNS@$_y$SiO$_2$/PDS system ([phenol]$_0$ = 0.50 mM; [PDS]$_0$ = 10.0 mM; [Ag(I)]$_0$ = 25 mM; [AuNS@$_y$SiO$_2$]$_0$ = 2.0 g/L; pH = 3.0; reaction time = 20 min).

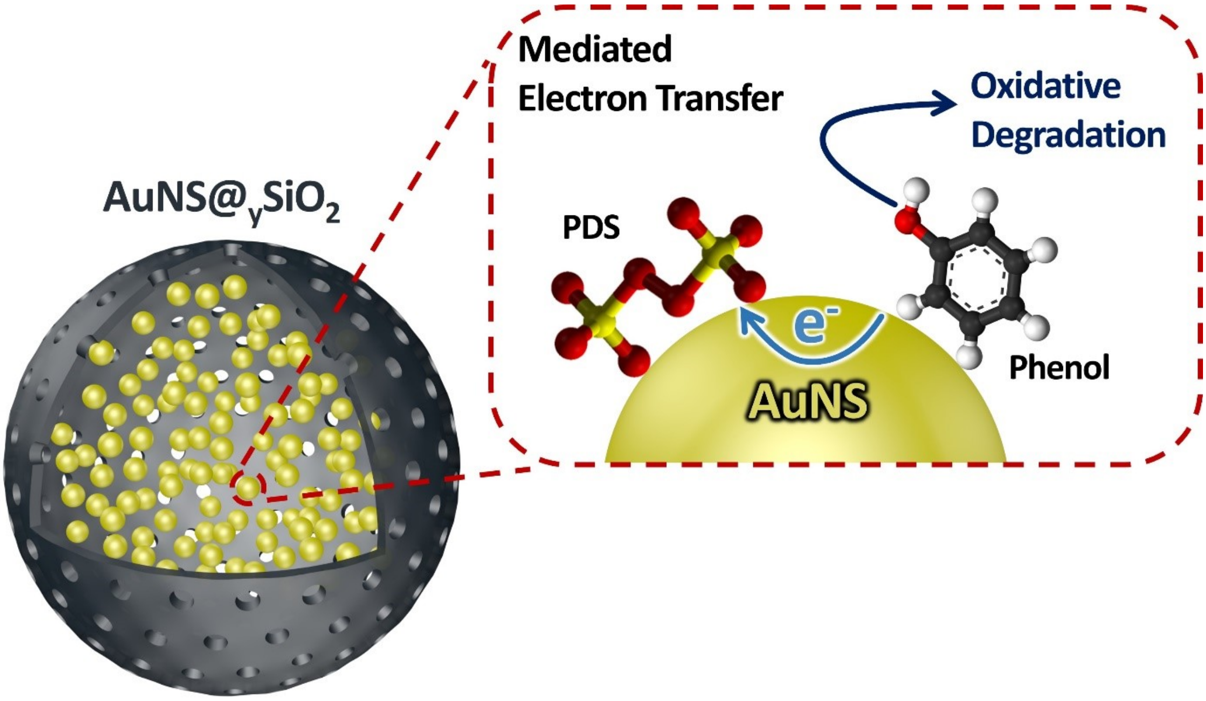

Fig. S8. Schematic illustration of nonradical pathway in the AuNS@$_y$SiO$_2$/PDS system.

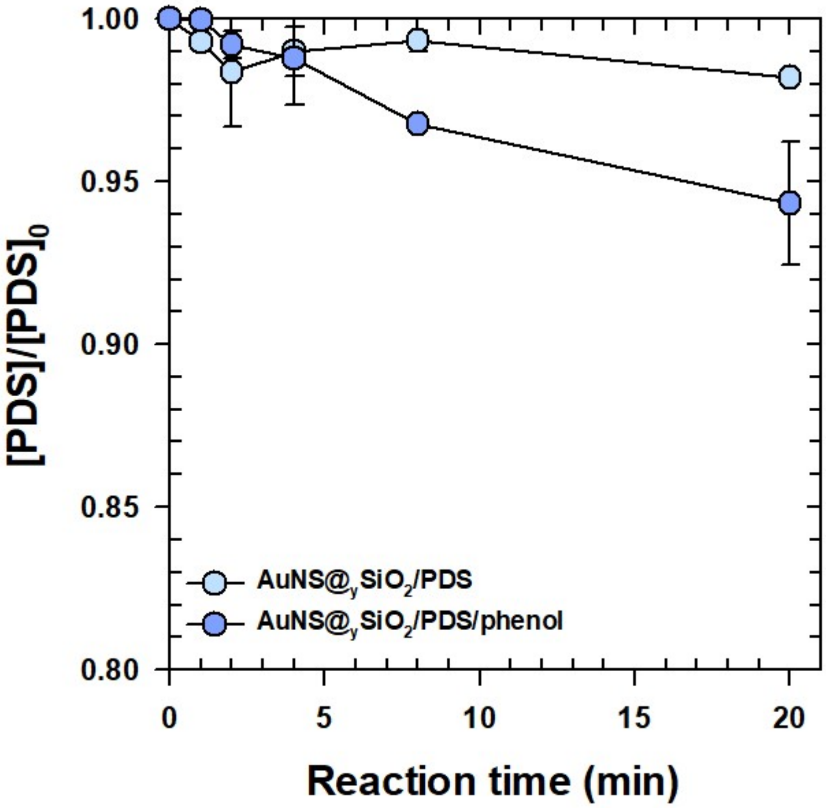

Fig. S9. Decomposition of PDS in the presence and absence of phenol in the AuNS@$_y$SiO$_2$/PDS system ([phenol]$_0$ = 0.50 mM; [PDS]$_0$ = 10.0 mM; [AuNS@$_y$SiO$_2$]$_0$ = 2.0 g/L; pH = 3.0; reaction time = 20 min).

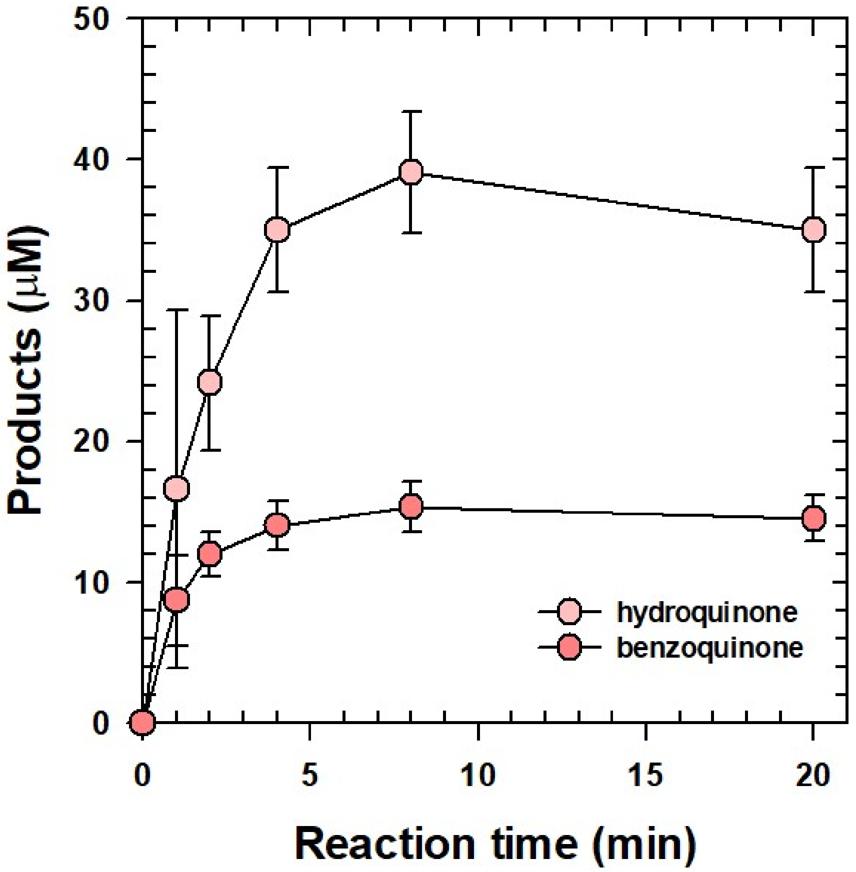

Fig. S10. Formation of hydroquinone and benzoquinone as phenol oxidation intermediates by the AuNS@$_y$SiO$_2$/PDS system ([phenol]$_0$ = 0.50 mM; [PDS]$_0$ = 10.0 mM; [AuNS@$_y$SiO$_2$]$_0$ = 2.0 g/L; pH = 3.0; reaction time = 20 min).

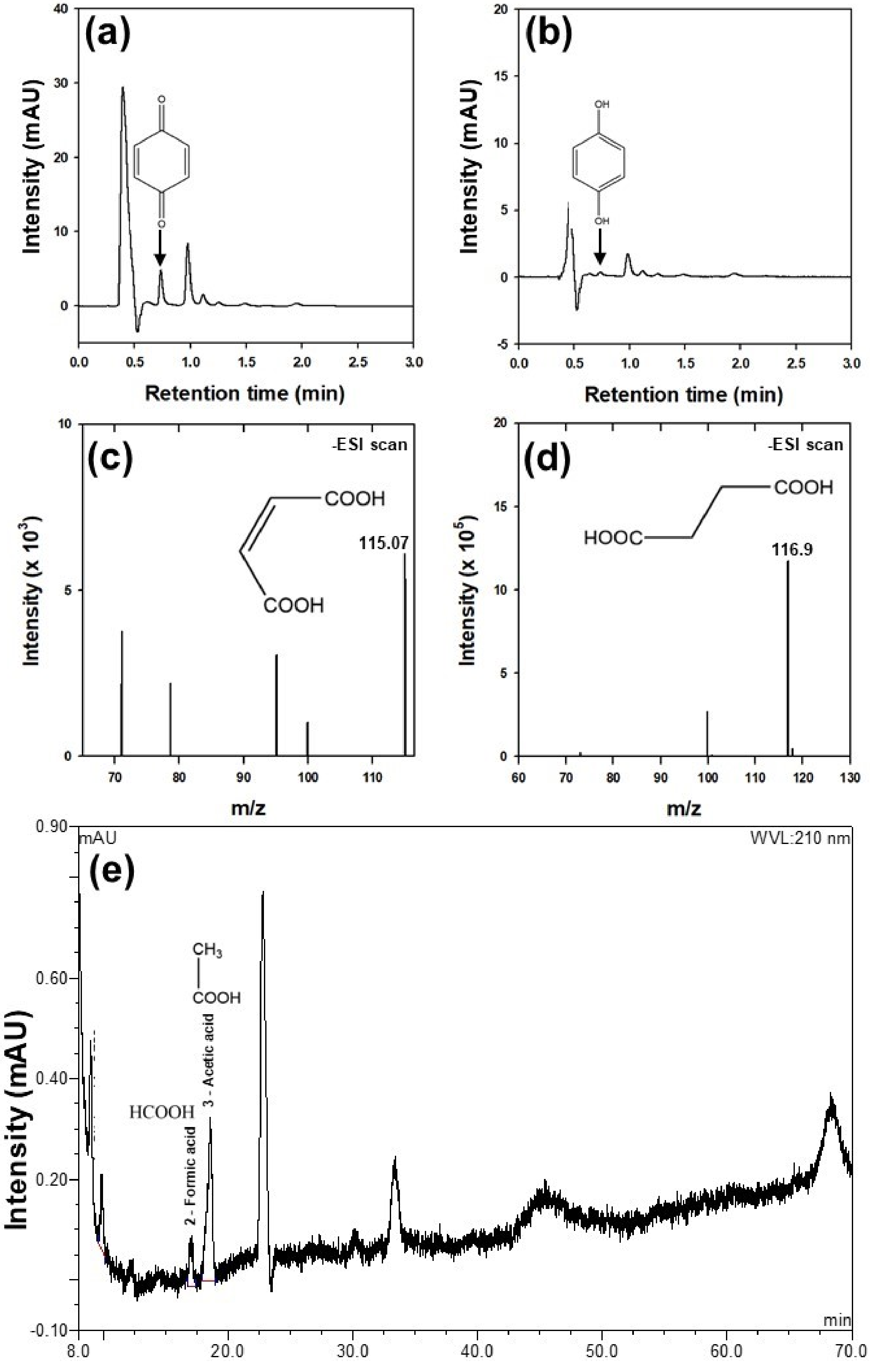

Fig. S11. RSLC spectra of (a) benzoquinone and (b) hydroquinone. LC/MS spectra of (c) maleic acid and (d) succinic acid. RSLC spectra of (e) formic acid and acetic acid.

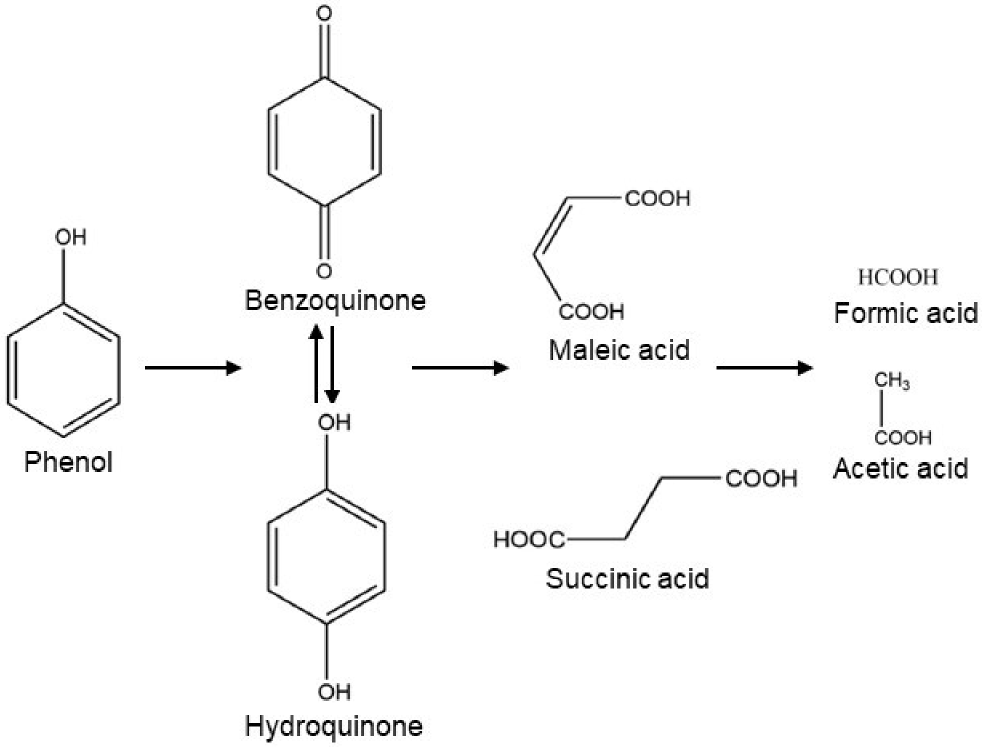

Fig. S12. Pathway of phenol degradation by the AuNS@$_y$SiO$_2$/PDS system.

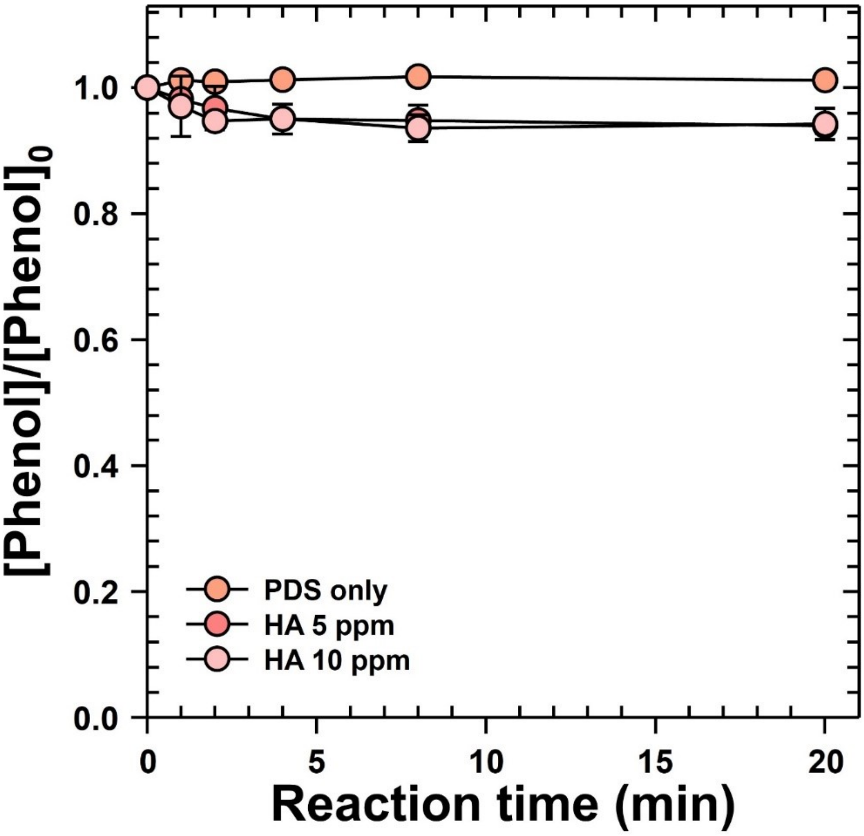

Fig. S13. Degradation of phenol in the presence of humic acid and PDS ([phenol]$_0$ = 0.50 mM; [PDS]$_0$ = 10.0 mM; [humic acid]$_0$ = 5, 10 ppm; pH = 3.0; reaction time = 20 min).

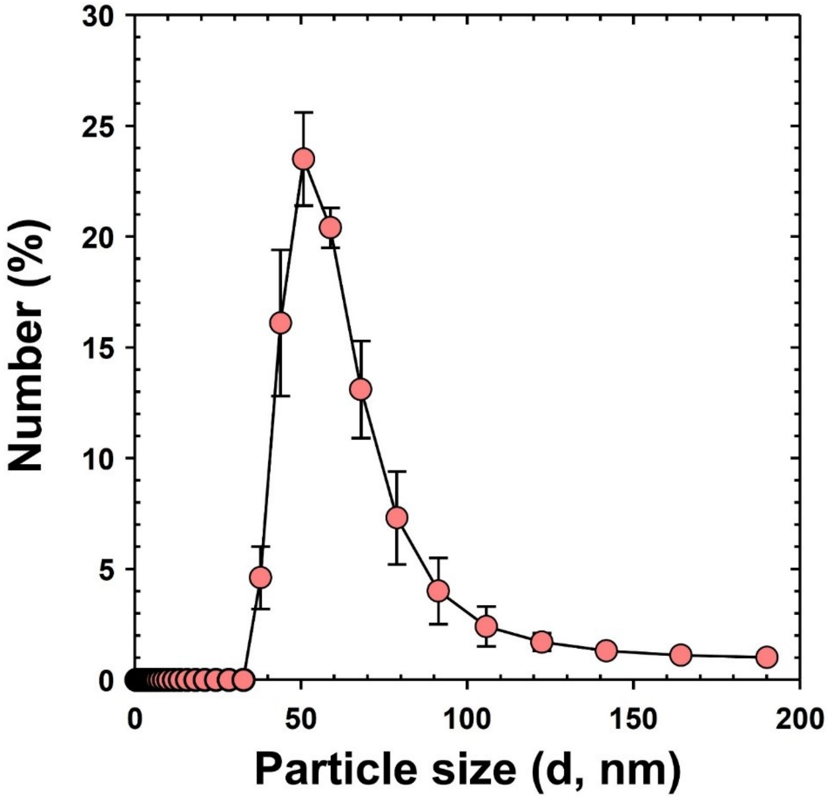

Fig. S14. Particle size distribution of humic acid ([humic acid]$_0$ = 10 ppm, pH = 3.0).

References

[S1] M. Zhang, C. Xiao, X. Yan, S. Chen, C. Wang, R. Luo, J. Qi, X. Sun, L. Wang and J. Li, Efficient removal of organic pollutants by metal–organic framework derived Co/C yolk–shell nanoreactors: size-exclusion and confinement effect, *Environ. Sci. Technol.*, 2020, **54**(16), 10289–10300.

[S2] T. Zeng, X. Zhang, S. Wang, H. Niu and Y. Cai, Spatial Confinement of a Co3O4 Catalyst in Hollow Metal–Organic Frameworks as a Nanoreactor for Improved Degradation of Organic Pollutants, *Environ. Sci. Technol.*, 2015, **49**(4), 2350–2357.

[S3] X. Zhang, X. Yan, X. Hu, R. Feng, M. Zhou and L. Wang, Efficient removal of organic pollutants by a Co/N/S-doped yolk-shell carbon catalyst via peroxymonosulfate activation, *J. Hazard Mater.*, 2022, **421**, 126726.

[S4] E. T. Yun, H. Y. Yoo, H. Bae, H. I. Kim and J. Lee, Exploring the role of persulfate in the activation process: radical precursor versus electron acceptor. *Environ. Sci. Technol.*, 2017, **51**(17), 10090–10099.

[S5] G. Xian, L. Niu, G. Zhang, N. Zhou, Z. Long, and R. Zhi, An efficient CuO-γFe2O3 composite activates persulfate for organic pollutants removal: Performance, advantages and mechanism, *Chemosphere*, 2020, **242**, 125191.

[S6] G. Xian, G. Zhang, H. Chang, Y. Zhang, Z. Zou, and X. Li, Heterogeneous activation of persulfate by Co3O4-CeO2 catalyst for diclofenac removal. *J. Environ. Manage.*, 2019, **234**, 265–272.

[S7] H. Lee, H. I. Kim, S. Weon, W. Choi, Y. S. Hwang, J. Seo, C. Lee and J. H Kim, Activation of persulfates by graphitized nanodiamonds for removal of organic compounds. *Environ. Sci. Technol.*, 2016, **50**(18), 10134–10142.

[S8] B. Yang, H. Kang, Y. J. Ko, H. Woo, G. Gim, J. Choi, J. Kim, K. Cho, E. J. Kim, S. G. Lee, H. Lee and J. Lee, Persulfate activation by nanodiamond-derived carbon onions: Effect of phase transformation of the inner diamond core on reaction kinetics and mechanisms. *Appl. Catal. B*, 2021, **293**, 120205.

[S9] G. Wang, L. Ge, Z. Liu, X. Zhu, S. Yang, K. Wu, P. Jin, X. Zeng and X. Zhang, Activation of peroxydisulfate by defect-rich CuO nanoparticles supported on layered MgO for organic pollutants degradation: An electron transfer mechanism. *Chem. Eng. J.*, 2022, **431**, 134026.

[S10] G. V. Buxton, C. L. Greenstock, C.L., W. P. Helman, and A. B. Ross, Critical Review of rate constants for reactions of hydrated electrons, hydrogen atoms and hydroxyl radicals (·OH/·O− in Aqueous Solution, *J. Phys. Chem. Ref. Data*, 1988, **17**(2), 513–886.

[S11] G. P. Anipsitakis, and D. D. Dionysiou, Radical generation by the interaction of transition metals with common oxidants, *Environ. Sci. Technol.*, 2004, **38**(13), 3705–3712.

[S12] P. Neta, V. Madhavan, H. Zemel, and R. W. Fessenden, Rate constants and mechanism of reaction of sulfate radical anion with aromatic compounds, *J. Am. Chem. Soc.*, 1977, **99**(1), 163–164.

[S13] L. Zhu, J. M. Nicovich, and P. H. Wine, Temperature-dependent kinetics studies of aqueous phase reactions of SO4− radicals with dimethylsulfoxide, dimethylsulfone, and methanesulfonate, *J. Photochem. Photobiol., A*, 2003, **157**(2–3), 311–319.

[S14] J. Ziajka, and W. Pasiuk-Bronikowska, Rate constants for atmospheric trace organics scavenging SO4− in the Fe-catalysed autoxidation of S (IV), *Atmos. Environ.*, 2005, **39**(8), 1431–1438.

[S15] F. E. Scully Jr, and J. Hoigné, Rate constants for reactions of singlet oxygen with phenols and other compounds in water, *Chemosphere*, 1987, **16**(4), 681–694.

[S16] J. A. Khan, X. He, N. S. Shah, H. M. Khan, E. Hapeshi, D. Fatta-Kassinos, and D. D. Dionysiou, Kinetic and mechanism investigation on the photochemical degradation of atrazine with activated H2O2, S2O82− and HSO5−, *Chem. Eng. J.*, 2014, **252**, 393–403.

[S17] M. M. Huber, S. Canonica, G. Y. Park, and U. Von Gunten, Oxidation of pharmaceuticals during ozonation and advanced oxidation processes, *Environ. Sci. Technol.*, 2003, **37**(5), 1016–1024.

[S18] M. M. Ahmed, S. Barbati, P. Doumenq, S. and Chiron, Sulfate radical anion oxidation of diclofenac and sulfamethoxazole for water decontamination, *Chem. Eng. J.*, 2012, **197**, 440–447.